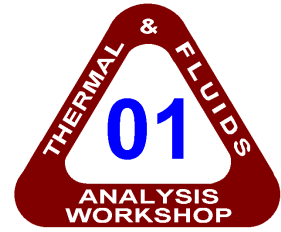


THERMAL RESPONSE MODELING SYSTEM FOR A MARS SAMPLE RETURN VEHICLE

Y.-K. Chen and F.S. Milos
Thermal Protection Materials & Systems Branch
NASA Ames Research Center, MS 234-1
Moffett Field, CA 94035-1000



ABSTRACT

A multi-dimensional, coupled thermal response modeling system for analysis of hypersonic entry vehicles is presented. The system consists of a high fidelity Navier-Stokes equation solver (GIANTS), a two-dimensional implicit thermal response, pyrolysis and ablation program (TITAN), and a commercial finite-element thermal and mechanical analysis code (MARC). The simulations performed by this integrated system include hypersonic flowfield, fluid and solid interaction, ablation, shape change, pyrolysis gas generation and flow, and thermal response of heatshield and structure. The thermal response of the heatshield is simulated using TITAN, and that of the underlying structural is simulated using MARC. The ablating heatshield is treated as an outer boundary condition of the structure, and continuity conditions of temperature and heat flux are imposed at the interface between TITAN and MARC. Aerothermal environments with fluid and solid interaction are predicted by coupling TITAN and GIANTS through surface energy balance equations. With this integrated system, the aerothermal environments for an entry vehicle and the thermal response of the entire vehicle can be obtained simultaneously. Representative computations for a flat-faced arc-jet test model and a proposed Mars sample return capsule are presented and discussed.

INTRODUCTION

Spacecraft heatshields typically use thermal protection system (TPS) materials that pyrolyze and ablate at high temperature for mass-efficient rejection of the aerothermal heat load. Pyrolysis is an internal decomposition of the solid that releases gaseous species, whereas ablation is a combination of processes that consume heatshield surface material (including chemical reactions, melting, and vaporization). For design and sizing of ablating spacecraft TPS materials, it is important to have a reliable numerical procedure that can predict surface recession rate, in-depth pyrolysis, and internal temperature history. The thermal properties and the boundary conditions of the heatshield also must be precisely defined to perform an accurate prediction.

A simplified schematic diagram of the geometry is shown in Figure 1. The outer face of the heatshield is exposed to an aerothermal heating environment that can be predicted using a high fidelity computational fluid dynamics (CFD) code with surface-thermochemistry boundary conditions. The inner face of the heatshield is attached to a structure that contains various other components. The structure often should be included in the thermal response simulation to correctly predict the bond-line temperature history. The maximum allowable bond-line temperature is typically the key parameter that drives the TPS thickness. The structure and its interior can have a complicated geometry, but the thermal response is relatively simple compared with that of the TPS.

A number of programs have been written to simulate ablating heatshields. The CMA code,¹ developed by Aerotherm Corporation in the 1960's, was one of the first one-dimensional codes. CMA solved internal energy balance and decomposition equations coupled with general surface energy balance boundary (SEB) conditions to simulate the response of pyrolyzing and ablating heatshields in hypersonic flows. In 1997, the FIAT code was developed at NASA Ames Research Center to support the development of lightweight ceramic ablaters. FIAT is numerically more stable and solves a wider range of problems than CMA, and it has been used for TPS sizing calculations in various NASA space missions.² However, the governing equations solved in both CMA and FIAT are one-dimensional. Thus, neither of these two codes is applicable for conditions in which a one-dimensional assumption is not true, such as the nose-tip of a slender hypersonic reentry vehicle or around the shoulder of a blunt vehicle.

For axisymmetric or planar geometries, Aerotherm also developed ASCC,³ an engineering code for fully-coupled fluid/solid simulation of ablating heatshields. In ASCC the thermal diffusion equation is solved using a finite-difference scheme with overlaid grids. A two-dimensional ablation code developed at Sandia National Laboratories uses the finite-control-volume method with unstructured grids.⁴ In this code, mesh motion (owing to ablation) is modeled by assuming the mesh behaves as a linear elastic solid. In both of these codes the effect of pyrolysis gas is not considered. Recently the TITAN program was developed to perform two-dimensional thermal response and shape change simulations for pyrolyzing ablaters.⁵ The governing equations, which include energy conservation and a three-component decomposition model with a moving grid, are discretized using a finite-volume approximation and general body-fitted coordinates. Time-accurate solutions are achieved by an implicit time marching technique using Gauss-Siedel line relaxation with alternating sweeps.⁶ In many cases, a coupled fluid and solid simulation is required for

accurate prediction of shape change, because shape change can not be correctly determined without appropriate aerothermal heating, but aerothermal heating is very sensitive to the geometry of the solid. To this end, the Navier-Stokes solver, GIANTS,⁷ was successfully coupled with TITAN using a loosely coupled method for simulating the fluid/solid interaction. TITAN uses an external zone with a moving grid and internal grid that is fixed. This two-zone approach can handle some simple geometries but is not sufficiently flexible to model a complicated interior structure.

To address this deficiency, the purpose of the present work is to integrate GIANTS and TITAN with the MARC finite-element code.⁸ The three codes are integrated through the use of MARC's user-supplied boundary condition subroutines. TITAN is used for the heatshield analysis because the physics of pyrolysis and ablation is too complicated for available commercial finite-element codes to accurately simulate. The structural materials beneath the heatshield experience relatively benign heat loads, and are usually multi-dimensional with complicated geometry. A commercial finite-element code, such as MARC, can perform thermal and structural analyses of the interior of a space vehicle. This integrated system can predict, simultaneously, two-dimensional aerothermal heating, ablation, shape change, and thermal response of heatshield and structure. The integrated simulation program should significantly reduce the computational and human effort required to design and analyze a spacecraft heatshield and attached structure. To demonstrate the capability of this modeling system, representative computations for an arc-jet model and a proposed Mars sample return capsule are presented and discussed.

INTEGRATED MODELING SYSTEM

Figure 2 presents the flow chart for integrated thermal response modeling system. The MARC, TITAN, and GIANTS codes are the three major components in the system. A brief description of each code is listed in the following subsections. The accuracy of each code has been studied previously.^{5,7,9} This modeling system is integrated around the MARC code. The front end of MARC, known as Mentat,¹⁰ is a graphical user interface program. The material properties are provided by TPSX,¹¹ a material properties database developed at NASA Ames Research Center.

MARC and TITAN are interfaced through MARC's heat-flux boundary condition routine. The continuity conditions of heat flux and temperature are imposed at the interface:

$$q_{MARC}^{l+1} = -k\nabla T|_{TITAN}^l \quad (1)$$

$$T_{TITAN}^{l+1} = T_{MARC}^l \quad (2)$$

At each time increment (from l to $l+1$) the front-face heat flux boundary condition of MARC is updated using the temperature gradient calculated by TITAN using Eq. (1), and the back-face temperature boundary condition of TITAN is equal to the temperature computed by MARC using Eq. (2) at each interface point.

TITAN and the flow environment code GIANTS are interfaced using MARC's surface energy balance boundary condition. The conditions at the ablating surface are determined by convective and radiative heating and by surface thermochemical interactions with the boundary layer gases. The SEB equation employed is of the convective transfer coefficient type and takes the form:¹²

$$\rho_e u_e C_h [H_r - (1 + B')h_w] + \dot{m}_c h_c + \dot{m}_{gw} h_{gw} + \alpha_w q_{Rw} - F\sigma\epsilon_w T_w^4 - q_{Cw} = 0 \quad (3)$$

The sum of the first three terms in Eq. (3) is the convective heat flux plus the heat of ablation. The fourth and fifth terms are the radiative heat fluxes absorbed and reradiated by the wall, respectively, and the last term represents the rate of conduction into material. Here B' is a nondimensionalized mass blowing rate. Tables of B' for charring materials can be generated using ACE¹³ or MAT.¹⁴

A blowing correction accounts for the reduction in transfer coefficients due to the transpiration or blowing effect of gases from pyrolysis and surface ablation being injected into the boundary layer. The blowing correction equation for convective heat transfer is:

$$\frac{C_h}{C_{h1}} = \frac{\ln(1 + 2\lambda B')}{2\lambda B'} \quad (4)$$

where λ is blowing reduction parameter and C_h/C_{h1} is the ratio of blown (ablating) to unblown (nonablating) heat transfer coefficients. With $\lambda = 0.5$, Eq.(4) reduces to the classical laminar-flow blowing correction.¹⁵ A variable λ is used for cases with transitional or turbulent flow.

The computation starts with the MARC code. At each time increment, MARC calls TITAN to compute a new heat flux boundary condition. At the same time TITAN obtains its back-face temperature boundary condition from MARC and, if necessary, calls the flow environment code to update the front-face SEB boundary condition. When the maximum local surface recession exceeds a predefined criterion since the last surface convective heating was calculated,

a new flow-field grid is generated based on the current body geometry, and the flow simulation routine is called to compute the aerothermal heating environment. Each call to the flow environment routine is a steady-state calculation. The non-ablating surface heating is calculated by the flow code, and the blowing reduction parameter is used in TITAN to take into account the laminar flow blockage due to surface blowing. As expected, the GIANTS calculation is much more computationally intensive than the thermal response computation. For a coupled GIANTS/TITAN/MARC simulation, most of the CPU time is consumed by flow environment calculations. Thus, the CPU time required for a simulation is primarily determined by the efficiency of the GIANTS code.

MARC

Structural material thermal response and thermal stress analysis are performed using the commercial finite-element code, MARC. The heat transfer and mechanical analyses can be coupled or performed separately. The internal energy conservation law is

$$\rho c_p \frac{\partial T}{\partial t} - \nabla \cdot (k \nabla T) = Q. \quad (5)$$

The boundary conditions include prescribed temperature, heat flux, and convective heat transfer coefficient to the environment. For transient analysis, the initial temperature is specified to start the calculation. To perform thermal stress analysis, MARC uses an instantaneous thermal expansion coefficient defined as

$$d\varepsilon_{kl}^{th} = \alpha_{kl} dT. \quad (6)$$

In most cases, however, thermal expansion data are given with respect to a reference temperature T_0 , as

$$\varepsilon^{th} = \bar{\alpha}(T - T_0). \quad (7)$$

Hence, the conversion of the expansion data to the instantaneous thermal expansion coefficient becomes

$$\alpha = \bar{\alpha} + \frac{d\bar{\alpha}}{dT}(T - T_0). \quad (8)$$

TITAN

Ablating heatshield thermal response and shape change computations are performed using TITAN. The governing equations include energy conservation and three-component decomposition model. The SEB condition, Eq. (3), is solved with a moving grid to calculate the shape change due to surface recession. The internal energy balance is a transient thermal conduction equation with additional pyrolysis terms:⁵

$$\rho c_p \frac{\partial T}{\partial t} = \nabla \cdot (k \nabla T) - (h_g - \bar{h}) \nabla \cdot \dot{m}_g + \dot{m}_g \cdot \nabla h_g + \dot{s} \rho c_p \nabla T \quad (9)$$

The individual terms in Eq. (9) may be interpreted as follows: rate of storage of sensible energy, net rate of thermal conductive heat flux, pyrolysis energy-consumption rate, net rate of energy convected by pyrolysis, and convection rate of sensible energy due to coordinate system movement.

A three-component decomposition model is used. The resin filler is presumed to consist of two components which decompose separately, while the reinforcing material is the third component which can decompose. The instantaneous density of the composite is given by:

$$\rho = \Gamma(\rho_A + \rho_B) + (1 - \Gamma)\rho_C \quad (10)$$

where A and B represent components of the resin, and C represents the reinforcing material. Γ is the volume fraction of resin and is an input quantity. Each of the three components can decompose following the relation:

$$\frac{\partial \rho_i}{\partial t} = -B_{ai} \exp\left(\frac{-E_{ai}}{RT}\right) \rho_{vi} \left(\frac{\rho_i - \rho_{ri}}{\rho_{vi}}\right)^{\Psi_i} + \dot{s} \nabla \rho_i, \quad i = A, B, C \quad (11)$$

where ρ_{vi} and ρ_{ri} are the original and the residual (or terminal) density, respectively, of component i . The motion of pyrolysis gas is assumed to be one-dimensional along the surface-normal (η) direction, and thus the pyrolysis gas mass flux is calculated using the following approximation:

$$\dot{m}_g A = -\int_{\eta_0}^{\eta} \left(\frac{\partial \rho}{\partial t}\right) A d\eta \quad (12)$$

The governing equations are discretized using a finite-volume approximation with a general body fitted coordinate system. A time accurate solution is achieved by the implicit time marching technique using Gauss-Siedel line relaxation with alternating sweeps. The computational grid is compressed during the course of computation to account for surface recession.

GIANTS

The flow simulation over a large angle blunt body is performed using a Navier-Stokes solver. The GIANTS code solves the time-dependent conservation equations of mass, momentum, and energy for chemical and thermal non-equilibrium flow-field. The species mass conservation equation is given by⁶

$$\frac{\partial \rho_j}{\partial t} + \frac{\partial}{\partial x_k} (\rho_j u_k) = - \frac{\partial}{\partial x_k} (\rho_j v_{jk}) + w_j, \quad (13)$$

the momentum conservation is written as

$$\frac{\partial}{\partial t} (\rho u_l) + \frac{\partial}{\partial x_k} (\rho u_l u_k) = - \frac{\partial \tau_{lk}}{\partial x_k}, \quad (14)$$

and the energy conservation as

$$\frac{\partial E}{\partial t} + \frac{\partial}{\partial x_k} ((E + p)u_k) = - \frac{\partial q_k}{\partial x_k} - \frac{\partial}{\partial x_k} (u_l \tau_{lk}) - \sum_j \frac{\partial}{\partial x_k} v_{jk} h_j. \quad (15)$$

The governing equations are discretized using a finite-volume method. The numerical method used to solve these discretized equations is exactly the same as that used in the TITAN code. This fully implicit, Gauss-Seidel line relaxation technique has been shown to yield steady-state results efficiently. A bifurcation diffusion model¹⁶ was also implemented in this version of GIANTS to correctly compute multi-species mass diffusion.

ARC JET TEST MODEL

The first test case is a simulation of the flat-faced cylindrical arc-jet test model shown in Figure 3. The TPS material is phenolic-impregnated carbon ablator¹⁷ (PICA) with a body radius of 3.81 cm and corner radius of 0.381 cm. The PICA is bonded to a piece of aluminum honeycomb structure, and this assembly is inserted into a copper model holder. The copper is protected from high temperature by a ring of TPS tile material (AETB) and disk of TPS blanket material (FRSI). The length of arc-jet heat pulse is 35 s. The TPS is sized to keep the structure below a specified temperature for several minutes.

The PICA material is divided into 2 computational zones. Zone I is the region right next to structural materials, where temperature should remain sufficiently low so that resin decomposition can be ignored. Zone II is the region directly exposed to hot arc-jet stream, where surface recession and pyrolysis gas effects must be considered in the simulation. PICA zone II is finite-volume meshed for TITAN; the rest of the model is finite-element meshed for MARC. Because a large subsonic region forms in front of the flat-faced cylinder, the flowfield is simulated using the Navier-Stokes solver GIANTS. The flow simulation is limited to the region in front of the PICA for simplicity. The exterior surfaces of the AETB and copper are assumed to be adiabatic.

Predicted heat flux distributions (from GIANTS) along the PICA surface at various times are presented in Figure 4, and the recession history (from TITAN) is shown in Figure 5. The predicted Mach contours at the beginning and the end of the heat pulse are depicted in Figure 6. Initially the heat flux is very high on the relatively sharp corner and significantly lower at the centerline. Therefore the ablation rate is highest near the corner, and the corner gradually rounds off. As the corner rounds, the bow shock moves closer to the surface, and consequently the heat flux around the stagnation region increases.

Fluid and solid temperature contours at 35 s are shown in Figure 7 (for clarity, different temperature scales are used for the fluid and solid). The maximum shock and solid temperature reaches about 6800 K and 2900 K, respectively. At 200 s there is no flowfield because the arc jet is turned off, so only the solid temperature is plotted. The PICA surface continuously cools down through surface radiation, and as heat is conducted into the model the maximum temperature is at an interior location. Thus, at 200 s the hottest spot (about 650 K) is located at a depth of about 0.6 cm from the front surface.

MARS SAMPLE RETURN VEHICLE

The second test case is simulation of a Mars sample return capsule. The purpose of the Mars Sample Return Mission is to return samples of material collected at Mars to Earth so that they can be studied here. The final phase of the

mission uses an Earth entry, descent, and landing capsule (Figure 8) that has a 0.9-m diameter, spherically blunted, 60° half-angle cone forebody.¹⁸ This Earth Entry Vehicle (EEV) is designed to transport the samples safely through the Earth's atmosphere to a recoverable location on the surface, while maintaining the Martian samples at a temperature below 323 K. To minimize system complexity and the number of potential failure modes, the EEV design relies on a non-parachuted capsule that decelerates solely by aerodynamic forces during entry. A passive energy-absorbing material is used to cushion the Mars samples from excessively large deceleration during landing. The assumed trajectory is shown in Figure 9. The entry velocity is 11.6 km/s at angle of -25°. Peak heating occurs at 17 s, and peak deceleration is about 130 g at 20 s. Ground impact ("landing") occurs at about 41 m/s at 360.5 s.

A complete Pro/E model of the EEV contained 57 different types of parts including numerous small, non-axisymmetric features such as antennas, bolts, cable connections, latches, springs, and vents.¹⁹ Suppression of these features resulted in the model, shown in Figure 8, that contains 19 axisymmetric parts and volumes. The samples are located in region 19 inside an aluminum sample canister, parts 13-14. This can is held within a titanium containment vessel, parts 15-16. This assembly resides in a spherical structure called the impact shell, parts 4-5. This shell is made of carbon-carbon composite, as is the rest of the vehicle substructure, parts 1-3. Volume 17 contains an energy absorbing composite structure that is assembled in a soccer-ball construction. The remainder of the vehicle interior is filled with various insulating materials, air gaps, and silicone rubber. The forebody heatshield is 1.2-cm thick chopped-molded and tape-wrapped carbon phenolic, and the aft heatshield is 1.0-cm thick SLA 561-V. Materials properties were obtained from NASA Langley and from the TPSX database.

The TITAN code is used for analysis of the heatshield materials only, and the rest of the vehicle is solved in MARC. The MARC material map is presented in Figure 10, and the three grids are illustrated in Figure 11. A very fine grid is needed in both the fluid and the solid to resolve the steep temperature gradients and complicated physics near the surface of the vehicle. A relatively coarser grid is adequate in the interior of the vehicle where temperature gradients are lower and time scales are longer.

Predicted forebody pressure distributions at selected times are shown in Figure 12. The peak pressure, which occurs at about 20 s, is about 1.15 atm. The pressure decreases gradually on the nose, with a slight minimum near the sphere-cone tangency point. The pressure increases slightly along the conical frustrum, then decreases rapidly as the flow accelerates around the shoulder of the vehicle. Predicted forebody convective heat flux distributions are presented in Figure 13. The heat flux decreases steadily, except for a local maximum near the shoulder during part of the trajectory. The peak heat convective flux is about 1.1 kW/cm² at 17 s. The stagnation point heat flux is shown in Figure 14. The vehicle decelerates rapidly owing to its bluntness, thus the heat pulse is fairly narrow, with 95% of the heating occurring in 14 s. The radiative heat flux over the forebody is estimated using the NOVAR code.²⁰ The peak radiative heat flux is about 0.22 kW/cm² at 16.4 s. The total heat load at the nose is about 9.2 kJ/cm² of which 8.5 kJ/cm² is convective and 0.7 kJ/cm² is radiative.

The forebody heat flux and pressure histories are imposed as boundary conditions of the integrated TITAN/MARC code. Owing to the large uncertainties in predicting afterbody heating, afterbody flowfields were not simulated using the Navier-Stokes solver. Instead, the heating is assumed to be uniform over the entire aft surface and equal to 5% of the time-dependent forebody stagnation point heating. This procedure is imprecise but possibly conservative in estimating the overall heat load experienced by the aft heatshield.

The blowing reduction parameter of 0.5 is used in the boundary conditions, Eqs. (3-4) for TITAN. Predicted peak surface temperature and total recession are shown in Figure 15. The peak temperature is 2500 to 3200 K over most of the forebody. However, the total recession is relatively low (under 1 mm) owing to the high density of the carbon phenolic heatshield. Because the surface recession is much smaller than the nose and shoulder radii, the effect of shape change on the aerothermal heating is insignificant for this problem. The surface and bond line temperatures in the TPS at the stagnation point are presented in Figure 16. The surface temperature increases with total heat flux, but after peak heating the temperature decreases more gradually by reradiation as heat is conducted back toward the surface from the interior of the TPS. The bond line temperature begins to rise at 50 s, and has reached 500 K at 300 s. The stagnation point blowing rates are shown in Figure 17. The carbon phenolic initially pyrolyzes in response to the aerothermal heating, then when the heat flux is sufficiently high, ablation also occurs.

In-depth temperature contours computed by TITAN and MARC at various times are presented in Figure 18. At 40 s, all the heat is contained within the heatshield. The peak surface temperature has cooled to 950 K, but the internal temperatures are unchanged from the assumed initial value of 250 K. At 100 s, most of the thermal energy is still confined within the heatshield, but some heat has penetrated into the forebody structure and foam insulations. At later times the TPS continues to cool by reradiation and conduction to the interior. The air gap at the nose is effective in preventing heat conduction, and the main conduction paths are along the skirt structure and through the body foam. A small amount of heat conduction through the aft TPS is also visible at the later times. At 500 s (if the vehicle is intact) the sample canister is safely below the design limit of 323 K.

The vehicle impacts the ground at about 360 s. Depending on the angle of the collision and the ground characteristics at the impact site, the containment vessel is displaced some distance through the energy absorbing material toward the nose structure, and other vehicle damage can occur as well. It is not obvious what assumptions are conservative for continuing the thermal analysis in the post-landing (pre-recovery) phase. Various scenarios can be simulated using MARC, including an impact simulation using assumed mechanical properties for the various materials. Future work will consider contact resistances between materials, and mechanical analyses such as calculation of thermal and deceleration stresses in the carbon-carbon structure.

CONCLUSIONS

A multi-dimensional fully coupled fluid/heatshield/structure thermal response modeling system has been developed. The system consists of a two-dimensional implicit thermal response and ablation program (TITAN), a commercial finite-element thermal and mechanical analysis code (MARC), and a high fidelity Navier-Stokes equation solver (GIANTS). This system can simultaneously predict aerothermal environments, heatshield ablation and shape change, and structural material thermal response for hypersonic entry vehicles as well as test models in hypersonic ground facilities. Representative computations for an arc-jet model and a proposed Mars sample return capsule were demonstrated. This integrated system can substantially reduce the computational effort required for multi-dimensional thermal analysis of ablative heatshield and structural materials, and thus should simplify the design cycle for future vehicles.

ACKNOWLEDGEMENTS

Ruth Amundsen and Robert Dillman at NASA Langley provided the Pro/E model for the EEV, an EEV material-properties spreadsheet, and other useful information. Joe Olejniczak at NASA Ames provided CFD and NOVAR results for the EEV trajectory.

REFERENCES

1. Moyer, C.B., and Rindal, R.A., "Finite Difference Solution for the In-Depth Response of Charring Materials Considering Surface Chemical and Energy Balances," Aerotherm Corporation, Mountain View, California, Final Report 66-7, Part II, March 1967 (also NASA CR-1061, June 1968).
2. Chen, Y.-K., and Milos, F.S., "Ablation and Thermal Analysis Program for Spacecraft Heatshield Analysis," *J. of Spacecraft and Rockets*, Vol. 36, No. 3, 1999, pp. 475-483.
3. Rafinejad, D., Dahm, T.J., Brink, D.F., Abbett, M.J., and Wolf, C.J., "Passive Nosedip Technology (Part II) Program, Volume II, Computer User's Manual: ABRES Shape Change Code (ASCC)" Report SAMSO-TR-77-11, Acurex Corp., Mountain View, CA, Oct. 1986.
4. Hogan, R.E., Blackwell, B.F. and Cochran, R.J., "Numerical Solution of Two-dimensional Ablation Problems Using the Finite Control Volume Method with Unstructured Grids," AIAA Paper 94-2085, June 1994.
5. Chen, Y.-K., and Milos, F.S., "Two-Dimensional Implicit Thermal Response and Ablation Program for Charring Materials on Hypersonic Space Vehicles," *J. of Spacecraft and Rockets*, Vol. 38, No. 4, 2001, in press.
6. Candler, G. V., "The Computation of Hypersonic Ionized Flows in Chemical and Thermal Nonequilibrium," AIAA Paper 88-0511, Jan. 1988.
7. Chen, Y.-K., Henline, W.D., "Analysis of Hypersonic Arcjet Flowfields and Surface Heating of Blunt Bodies," AIAA Paper 93-0272, Jan. 1993.
8. Anon., *Users Manual, MARC Analysis Research Corporation, Volume A: Users Information*, MARC Analysis Research Corporation, Palo Alto, CA, 1994.
9. Chen, Y.-K., Milos, F.S., Bull, J.D., and Squire, T.H., "Integrated Analysis Tool for Ultra-High Temperature Ceramic Sharp-Body Reentry Vehicles," AIAA Paper 99-0350, Jan. 1999.
10. Anon., "Users Manual, Mentat II," MARC Analysis Research Corporation, Palo Alto, CA, 1995.
11. Squire, T.H., Milos, F.S., Hartlieb, G.C., and Rasky, D.J., "TPSX: Thermal Protection Systems Expert and Material Properties," *ICCE Fourth International Conference on Composites Engineering*, edited by D. Hui, ICCE and College of Engineering, University of New Orleans, July 1997, pp. 937-938.
12. Anon., *User's Manual: Aerotherm Charring Material Thermal Response and Ablation Program*, Report UM-87-11/ATD, Acurex Corporation, Mountain View, CA, Aug. 1987.

13. Anon., *User's Manual: Aerotherm Chemical Equilibrium Computer Program*, Report UM-81-11/ATD, Acurex Corporation, Mountain View, CA, Aug. 1981.
14. Milos, F.S., and Chen, Y.-K., "Comprehensive Model for Multi-Component Ablation Thermochemistry," AIAA Paper 97-0141, Jan. 1997.
15. Kays, W.M., and Crawford, M.E., *Convective Heat and Mass Transfer*, 2nd Edition, McGraw-Hill, 1980, pp. 355-357.
16. Bartlett, E.P., Kendal, R.M., and Rindal, R.A., "An Analysis of the Coupled Chemically Reacting Boundary Layer and Charring Ablator: Part IV – A Unified Approximation for Mixture Transport Properties for Multi-component Boundary-Layer Applications," NASA CR-1063, June 1968.
17. Tran, H., Johnson, C, Rasky, D., Hui, F., Chen, Y.-K., and Hsu, M., "Phenolic Impregnated Carbon Ablators (PICA) for Discovery Class Missions," AIAA Paper 96-1911, June 1996.
18. Mitcheltree, R.A., Braun, R.D., Hughes, S.J., and Simonsen, L.C., "Earth Entry Vehicle for Mars Sample Return," IAF Paper IAF-00-Q.3.04, Oct. 2000.
19. Amundsen, R.M., Dec, J.A., and Lindell, M.C., "Thermal Analysis Methods for an Earth Entry Vehicle," Eleventh Thermal and Fluids Analysis Workshop, Cleveland, OH, Aug. 2000.
20. Olynick, D.R., Henline, W.D., Chambers, L.H., and Candler, G.V., "Comparison of Coupled Radiative Navier-Stokes Flow Solutions with the Project Fire II Flight Data," AIAA Paper 94-1955, June 1994.

NOMENCLATURE

A	= area, m^2	u	= velocity, m/s
B'	= $\dot{m} / \rho_e u_e C_h$, nondimensional mass flux	v	= diffusion velocity, m/s
B_a	= pre-exponential constant in Eq.(11), s^{-1}	w	= mass source term, kg/m^3
C_h	= Stanton number for heat transfer	x	= general coordinate variable, m
c_p	= heat capacity, J/kg-K	α	= surface absorptance
E	= internal energy in Eq.(15), J/kg	$\bar{\alpha}$	= thermal expansion coefficient, 1/K
E_a	= activation energy in Eq.(11), J/kmol	ε	= surface emissivity
F	= view factor	ε^{th}	= thermal strain
g	= Earth standard gravity, 9.81 m/s^2	Γ	= volume fraction of resin
H_r	= recovery enthalpy, J/kg	λ	= blowing reduction parameter
h	= enthalpy, J/kg	ρ	= total density, kg/m^3
\bar{h}	= partial heat of charring in Eq.(9), J/kg	σ	= Stefan-Boltzmann constant, W/m^2-K^4
k	= thermal conductivity, W/m-K	τ	= CFD shear stress, N/m^2
\dot{m}	= mass flux, kg/m^2-s	Ψ	= decomposition reaction order
p	= pressure, N/m^2	η	= surface -normal coordinate, m
Q	= heat source term, J/m^3	subscripts	
q	= heat flux, W/m^2	c	= char
q_C	= conductive heat flux, W/m^2	e	= boundary-layer edge
q_R	= radiative heat flux, W/m^2	g	= pyrolysis gas
R	= universal gas constant, J/kmol-K	i	= density component (A, B, and C)
R_b	= maximum body radius, m	j	= gas phase species
R_c	= corner radius, m	k, l	= coordinate directions
R_n	= nose radius, m	v	= virgin
s	= stream length, m	w	= surface
\dot{s}	= surface recession rate, m/s	0	= reference value
T	= temperature, K	superscript	
t	= time, s	ℓ	= time level index

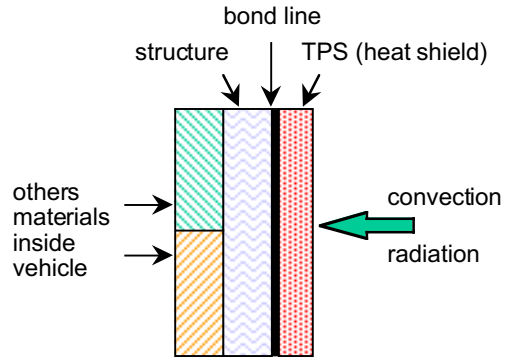


Figure 1. Schematic diagram of thermal analysis problem for a space vehicle.

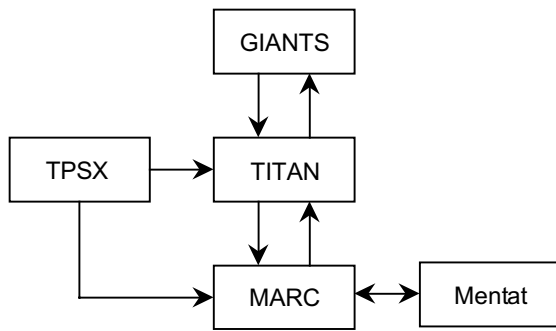


Figure 2. Flow chart for integrated thermal response modeling system.

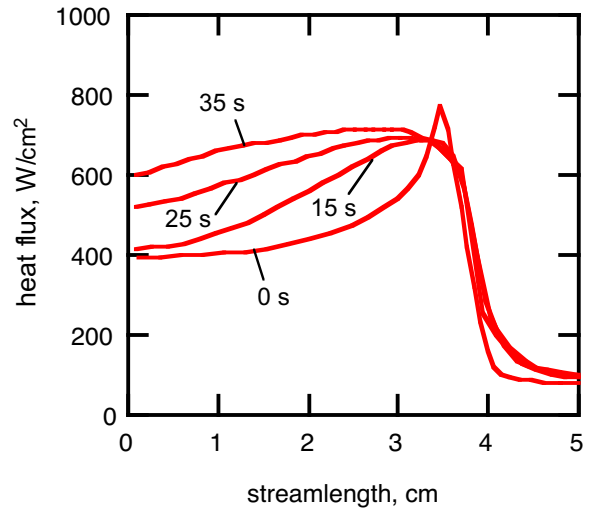


Figure 4. Heat flux on arc-jet model at various times.

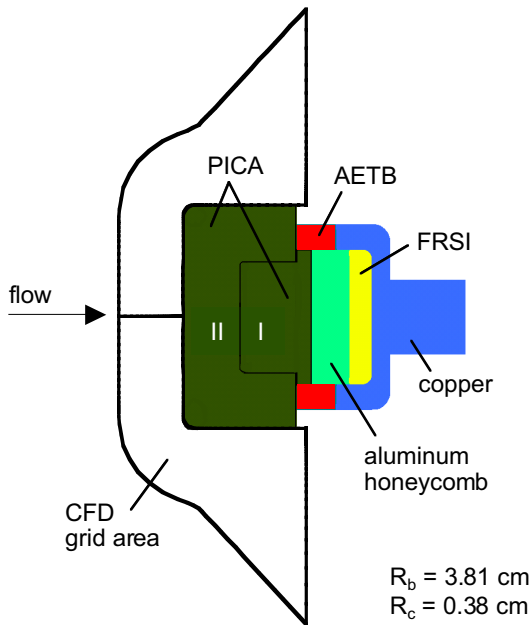


Figure 3. Flat faced arc-jet test model geometry.

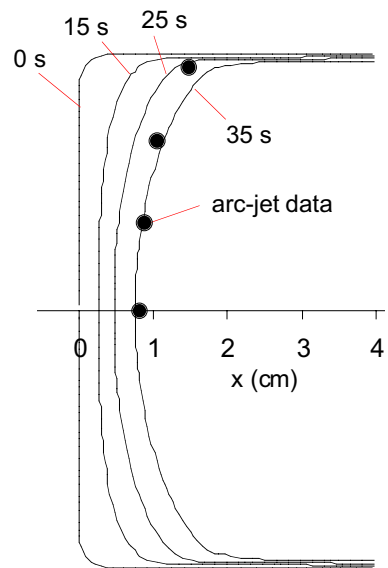


Figure 5. Recession history of arc-jet model.

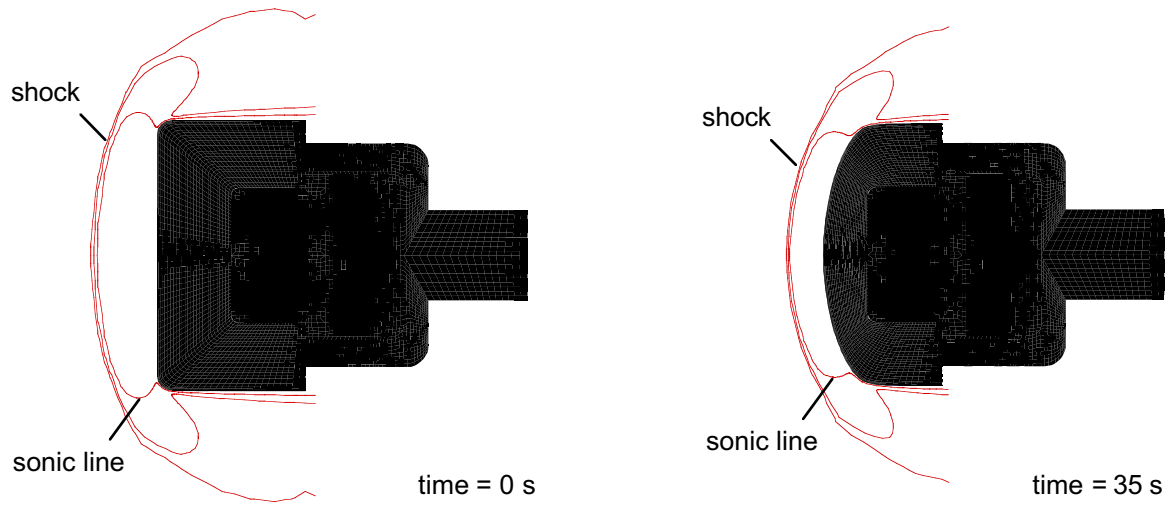


Figure 6. Mach contours for flow past arc-jet model at beginning (0 s) and end (35 s) of heating.

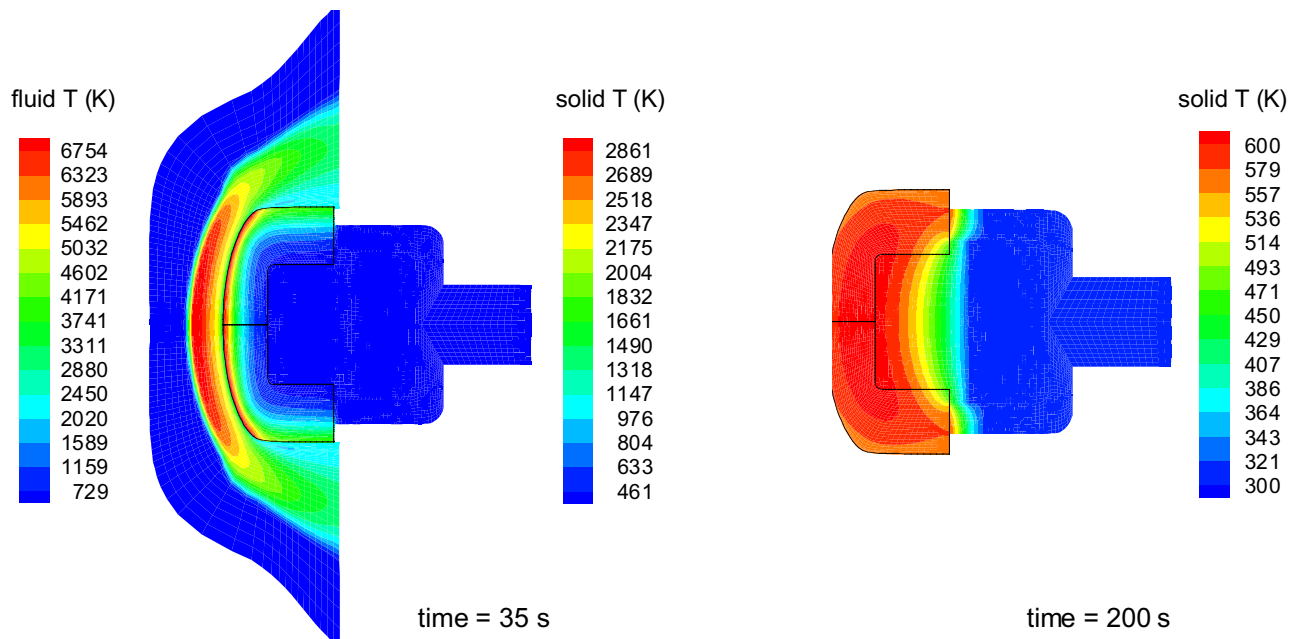


Figure 7. Temperature contours for arc-jet model.

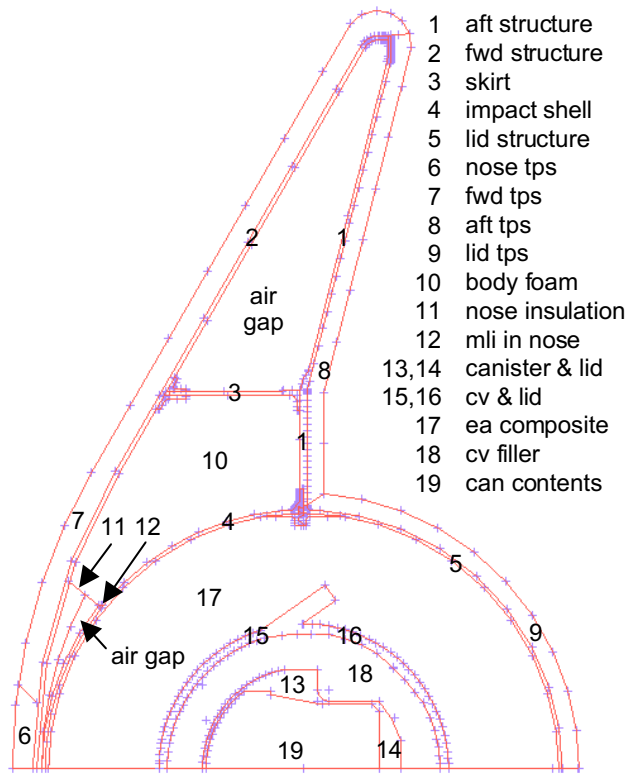


Figure 8. Axisymmetric EEV geometry.

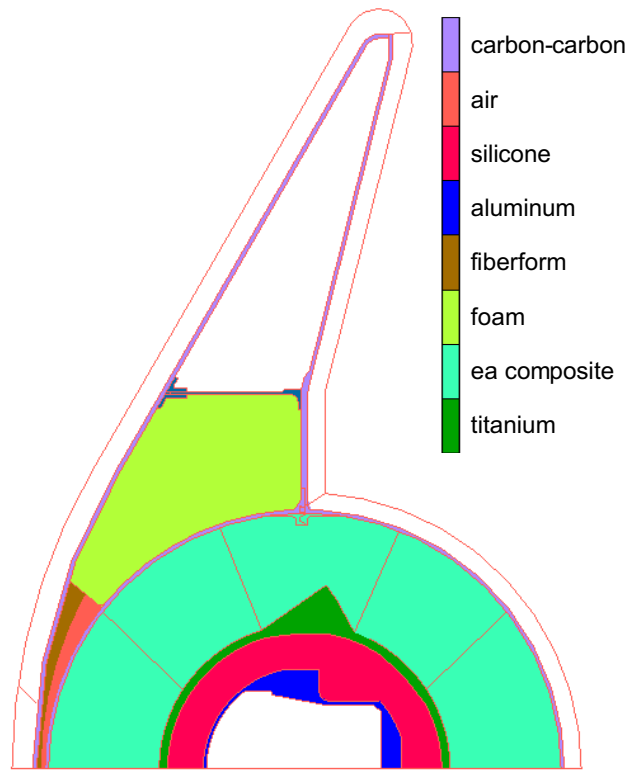


Figure 10. MARC geometry and material map.

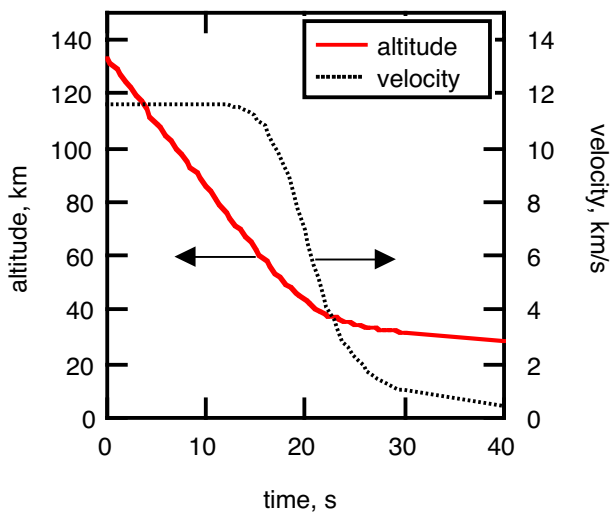


Figure 9. EEV trajectory.

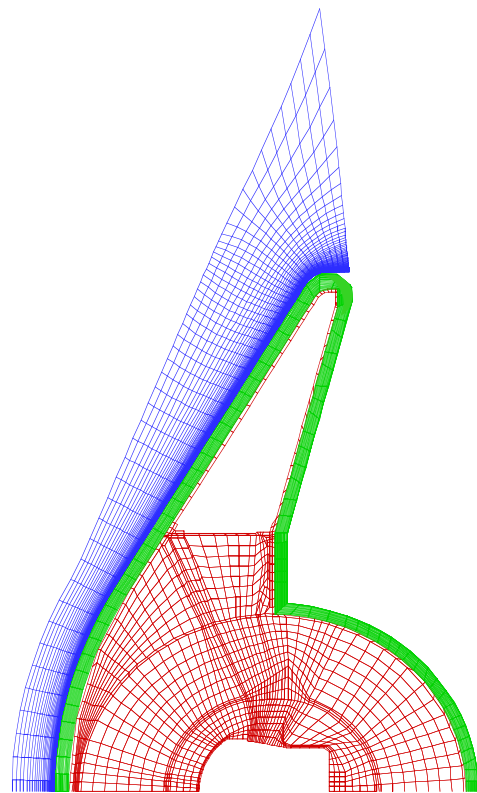


Figure 11. GIANTS grid (blue), TITAN grid (green), and MARC grid (red).

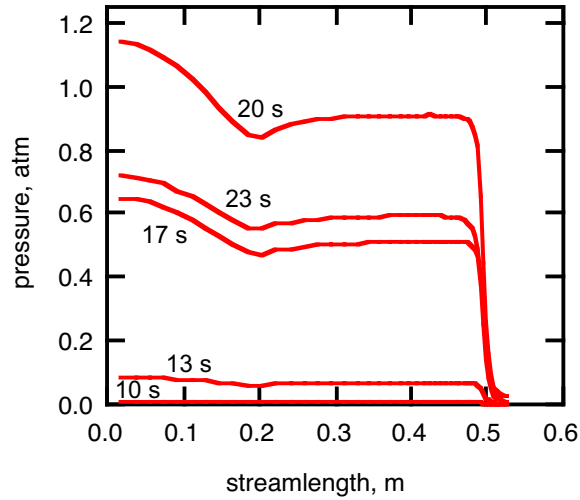


Figure 12. Surface pressure distribution at selected times.

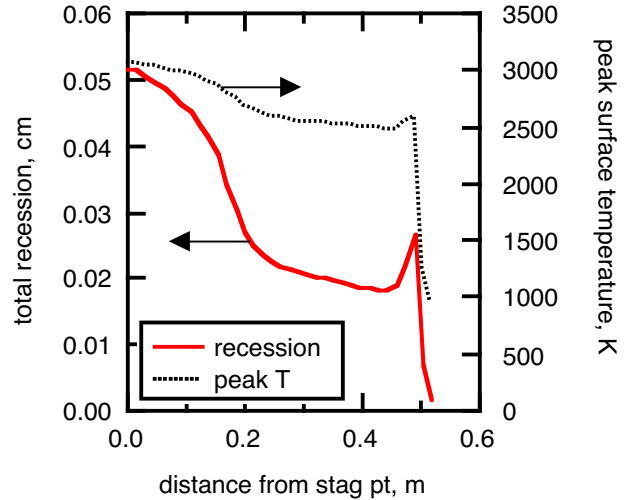


Figure 15. Surface peak temperature and recession.

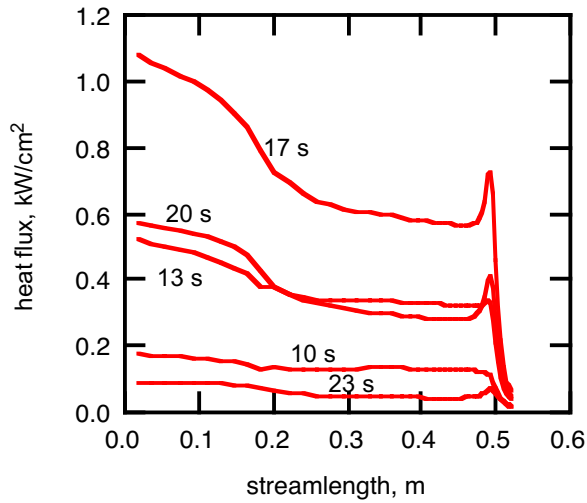


Figure 13. Surface heat flux distribution at selected times.

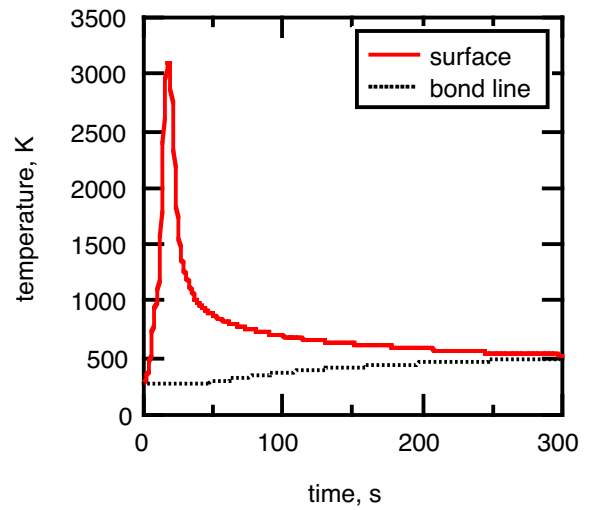


Figure 16. TPS temperature histories at stagnation point.

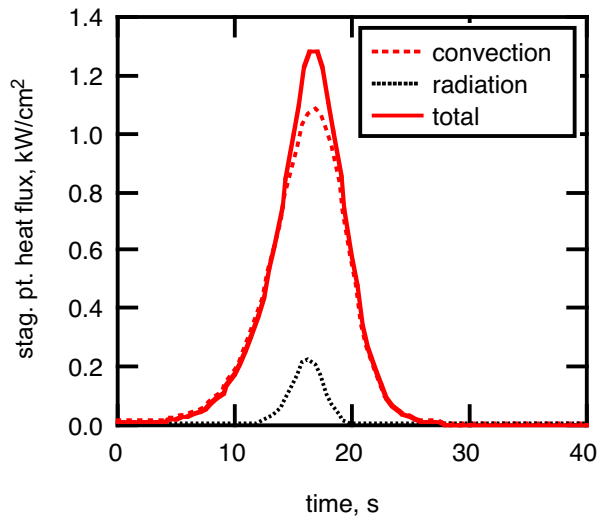


Figure 14. Stagnation point heat flux.

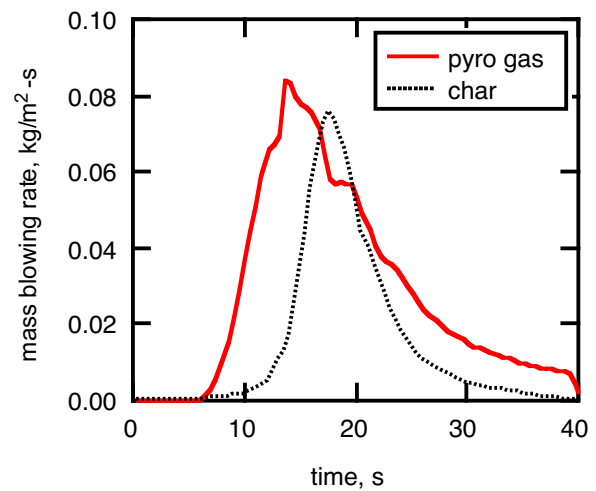


Figure 17. Surface mass flux at stagnation point.

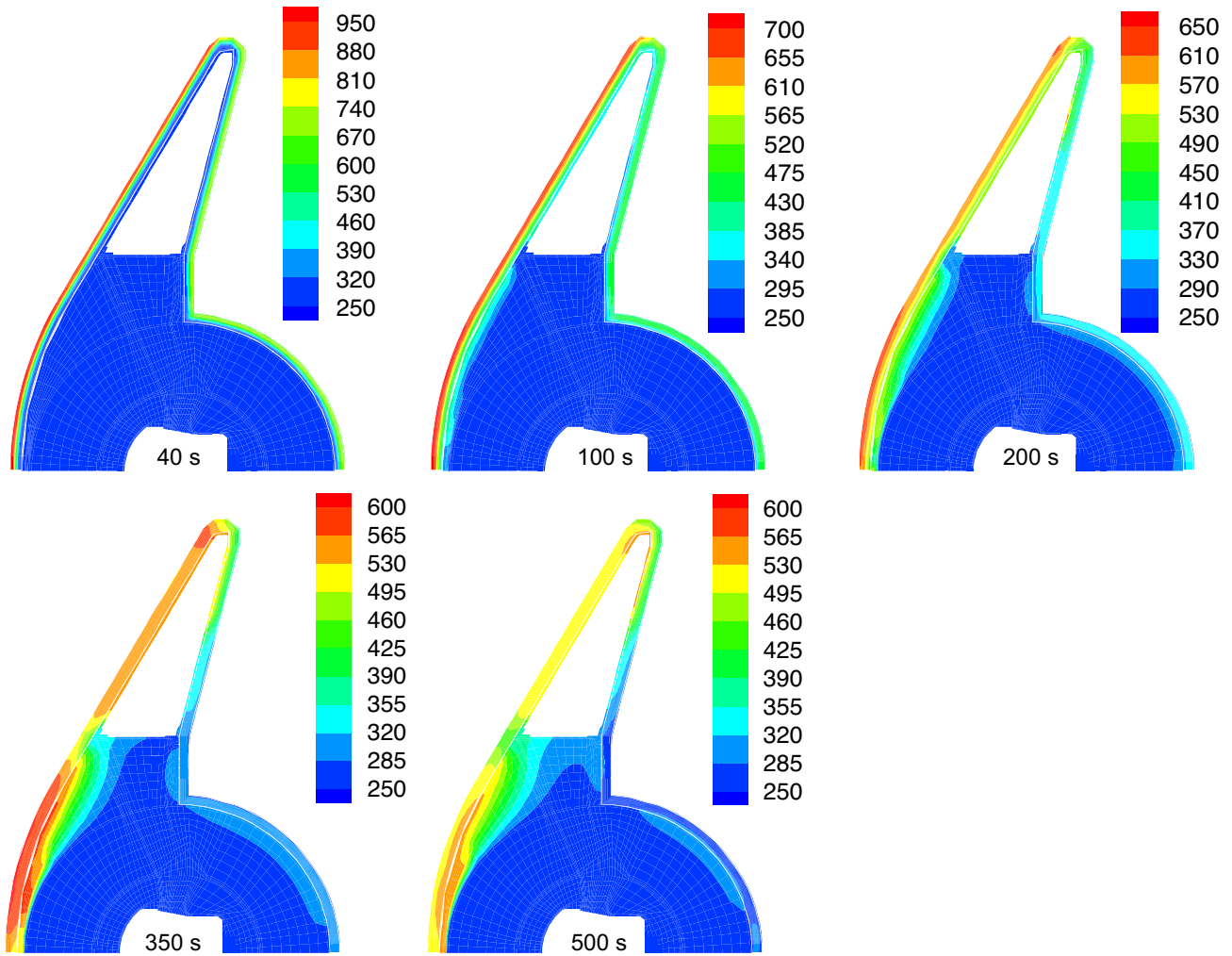


Figure 18. EEV temperature contours at selected times, K.